

Article

Microstructure, Microhardness, and Wear Properties of Cobalt Alloy Electrodes Coated with TiO₂ Nanoparticles

Sebastian Balos ^{1,*}, Petar Janjatovic ^{1,*} , Miroslav Dramicanin ¹ , Danka Labus Zlatanovic ¹, Branka Pilic ², Pavel Hanus ³ and Lucyna Jaworska ⁴

¹ Faculty of Technical Sciences, University of Novi Sad, 21000 Novi Sad, Serbia; dramicanin@uns.ac.rs (M.D.); danlabus@uns.ac.rs (D.L.Z.)

² Faculty of Technology, University of Novi Sad, 21000 Novi Sad, Serbia; brapi@uns.ac.rs

³ Department of Material Science, Technical University of Liberec, Liberec 461 17, Czech Republic; Pavel.Hanus@tul.cz

⁴ Lukasiewicz- Research Network-Institute of Advanced Manufacturing Technology, Centre for Materials Research and Sintering Technology, 30-011 Krakow, Poland; lucyna.jaworska@ios.krakow.pl

* Correspondence: sebab@uns.ac.rs (S.B.); janjatovic@uns.ac.rs (P.J.);
Tel.: +381-21-485-2339 (S.B.); +381-21-485-2323 (P.J.)

Received: 27 September 2019; Accepted: 23 October 2019; Published: 4 November 2019



Abstract: In this paper, the influence of TiO₂ nanoparticle coating on cobalt-based electrodes was studied. Different coating treatment times were applied, and the results were compared to the hard-faced layer obtained with unmodified electrodes. The hard facing was done in three layers, the first being a Ni-based interlayer, followed by two layers of corrosion and wear-resistant Co-based Stellite 6 alloy. Pin-on-disc wear testing was applied, along with the metallographic study and hardness measurements of the hard-faced layers. Furthermore, energy-dispersive X-ray spectroscopy (EDS) analysis was conducted. It was found that the microstructural properties, as well as microhardness profiles, are modified in hard-faced layers obtained with modified electrodes. Interdendritic distances are altered, as are the dendrite growth directions. Titanium oxides are formed, which, along with the present complex carbides, increase the wear resistance of the hard-faced layers compared to layers obtained with untreated electrodes.

Keywords: hard facing; cobalt alloys; wear; nano-particle coating

1. Introduction

Cobalt-based alloys, commonly known as Stellites, are well-known wear and corrosion resisting alloys [1]. Stellites are Co-Cr-W-C alloys, containing around 30% chromium and 4% to 14% tungsten, while some alloys have their tungsten replaced with molybdenum for increased resistance to reductive media. Also, they contain up to around 2.5% of carbon, to form wear-resisting complex carbides [2–5]. Stellite alloys properties are the result of the combined effects of the relatively ductile Co-based matrix that supports relatively hard carbides, providing wear resistance at both room and elevated temperatures up to 600 °C [6,7]. The matrix is based on chromium and tungsten solid solution in cobalt, while the carbides are of complex nature, predominantly of the chromium-rich M₇C₃ eutectic type [8]. There is a variety of Stellite alloys, suited to various environments and applications [3]. Major Stellite alloys, their chemical composition, hardness, and applications are presented in Table 1.

Table 1. Major Stellite alloys with their chemical composition, hardness, and applications [9,10].

Alloy	Co	Cr	W	C	Ni	Mo	Fe	Si	HRC	Properties	Applications
Stellite 1	Base	31	12	2.45	<3.0	<1.0	<3.0	<2.0	51–56	Erosion, abrasion resistance, crack sensitive	Valve seat inserts, bearings, cutter edges
Stellite 6	Base	29	4	1.2	<3.0	<1.0	<3.0	<2.0	39–43	General purpose wear, impact, cavitation resistance	Valve seats and gates, pump shafts and bearings, erosion shields, rolling couples
Stellite 12	Base	30	8	1.55	<3.0	<1.0	<3.0	<2.0	45–50	High temperature and corrosion resistance, properties between Stellite 1 and 6	Control plates, pump vanes, bearing bushes, narrow neck glass mold plungers, hard facing of engine valves, pinch rollers and rotor blade edges
Stellite 20	Base	32	16	2.45	<3.0	<1.0	<3.0	<2.0	53–57	High abrasion, good corrosion resistance and low shock resistance.	Pump sleeves, rotary seal rings, wear pads, bearing sleeves, centerless grinder work rests
Stellite 21	Base	28	-	0.25	3	5.5	<3.0	<1.5	27–40	Thermal, mechanical shock, cavitation resistance, not for abrasion	Building of forging and hot stamping dies
Stellite 25	Base	20	14	0.1	10	<1.0	<3.0	<1.0	20–45	Metal-on-metal wear, thermal fatigue, hot corrosion	Piercing points, forming tools, extrusion dies, furnace hardware

The most common alloy is Stellite 6, owing this to its relatively balanced properties. It is sometimes regarded to be the standard Stellite alloy, with good wear resistance, corrosion, cavitation erosion, ductility and heat resistance, retaining these properties up to approximately 500 °C. The main corrosion mechanism is pitting, and it is well suited to be used in chloride solutions and seawater, where weight loss is usually under 0.05 mm per year at 22 °C [11]. More recently, Marques et al. [12] studied the application of Stellite alloys for fabricating of the components used in the production of second-generation ethanol. In such devices, biomass containing around 8% abrasive particles is loaded into the reactor, along with sugar cane biomass. To achieve improved abrasive wear properties, an increase in molybdenum content was proposed [13], due to the formation of reinforcing Co₃Mo intermetallic compounds. However, molybdenum is a critical raw material (CRM) for the European Union. In addition to this, cobalt, tungsten, and silicon metal are all CRMs. Finally, Stellites contain chromium, that is near-CRM and nickel that is not CRM, but it is a relatively expensive metal [13,14]. That means, there is a considerable interest in increasing the life of Stellite components, to spare CRMs as much as possible. An alternative to adding molybdenum, and a possible way of increasing the life of Stellite components, is to enhance their wear properties. One of the potentially attractive ways of increasing the properties of the hard-faced layers made of Stellite 6 alloy is the introduction of TiO₂ nanoparticles into the existing electrode as proposed in [15–17]. In [15–17], where cellulose and rutile coated electrodes were modified by infiltrated TiO₂, this influenced the increased mechanical properties of the joints. In these studies, it was demonstrated that the addition of TiO₂ resulted in the increase in the number of complex Ti-Mn-Si oxide inclusions, acting as inoculants. That influenced the fine-grained acicular ferrite instead of Widmastaetten ferrite, which caused the increase in mechanical properties [15–17].

The aim of this study is to explore the influence of nanoparticles introduced on the Co-based hard-facing electrode with different immersion times on the wear resistance of the resulting hard-faced layer. The hard-faced layer was produced using the common shielded metal arc welding (SMAW) technique.

2. Materials and Methods

The SMAW (Shielded metal arc welding) process was used for hard facing. The base metal was S235JR, having the chemical composition shown in Table 2. Two types of hard-facing electrodes were used. The interlayer or buttering layer was done by Boehler Fox Nibas 70/20 (Boehler, Hamm, Germany; AWS A5.11-05: E NiCrFe-3) electrode in one pass. The final hard-faced layer was done by Co-based FSH Selectarc Co6, (Forges de Saint-Hippolyte, Roche-lez-Beaupre, France; Stellite 6; AWS A5.13: E CoCr-A) in two layers. Chemical compositions of the interlayer and hard-facing layer are presented in Tables 3 and 4. The overall thickness of the hard-faced layer was approximately 5 mm. The hard-facing parameters were in accordance with the electrode manufacturer's instructions (Table 5) and welding was done on an Iskra E10 (Iskra, Ljubljana, Slovenia) SMAW device.

Table 2. Chemical composition of S235JR (wt. %).

C	Si	Mn	S	Cr	P	Al	Cu	Mo	Ni	Fe
0.09	0.14	0.02	0.041	0.001	0.011	0.006	0.39	0.011	0.07	balance

Table 3. Nominal chemical composition of interlayer electrode AWS A5.11-05: E NiCrFe-3 (wt. %).

C	Si	Mn	Cr	Fe	Mo	Nb	Co	Ni
0.025	0.4	5.0	19.0	3.0	1.2	2.2	0.08	balance

Table 4. Nominal chemical composition of Co-based electrode AWS A5.13: E CoCr-A (wt. %).

C	Si	Cr	W	Fe	Co
1.1	1.0	28.0	4.5	3.0	balance

Table 5. Welding parameters.

Electrode Core Diameter × Length	Ø 3.2 × 450 mm
Current type	DC+
Welding current	85 A
Welding voltage	22 V
Welding speed	12 cm/min
Electrode inclination along welding direction	60°

TiO₂ nanoparticles were introduced in the form of a coating on the hard-facing Co-based electrode. The distilled water solution of 20 nm hydrophilic TiO₂ nanoparticles (5 wt. %) was placed into the EMAG Emmi-5 (Emmi Ultrasonic, Moerfelden-Walldorf, Germany) ultrasonic bath, along with the fully submerged electrodes. Three immersion times were used: 1, 5, and 10 min, resulting in hard-faced specimens designated as 2, 3, and 4. These hard-faced layers were compared to the layer obtained with the untreated electrode (hard-faced specimen 1). After such treatment, the electrodes were dried for 1 h at 250 °C. Overall, four hard-faced specimens were prepared, which were water jet cut into Ø 10 mm specimens. One specimen was square, 30 mm wide, and used for metallographic examination and hardness measurement on its cross-section.

The pin-on-disc wear test was done on a customized Struers DP-U2 (Struers, Bellerup, Denmark) laboratory-polishing machine, with the polishing wheel replaced with SiC grinding paper. Three FEPA (Federation of European Producers of Abrasives) grit sizes were used: P240 (44.5–110 µm SiC grains, median grain size 58.5 µm, according to ISO 6344-1), P360 (29.6–87 µm, median grain size 40.5 µm) and P500 (21.5–77 µm, median grain size 30.2 µm). Three loadings were used: 700 g, 1000 g, and 1300 g. The specimens were placed into the brass holder and mounted in a Struers PdM-Force (Struers, Bellerup, Denmark) specimen mover. Prior to each wear test, the specimens were ground with P2000 SiC abrasive paper. The wheel spindle speed was 250 min⁻¹, wear time was 60 s, and

the specimen axis was 70 mm away from the center of the spindle. During the wear test, a constant water flow of 100 mL/min was maintained, with a water temperature of 15 °C. The wear mass loss was reported for each test, with the mass of each specimen before and after wear measured by Tehnica Type 2615 (Tehnica, Zelezniki, Slovenia) analytic weight, having the accuracy of 0.1 mg. The results reported were calculated as an average of three specimens.

The metallographic characterization was conducted with a Leitz-Orthoplan (Leica-Leitz, Wetzlar, Germany) light microscope. Prior to this, the specimens were mounted, ground with abrasive papers (P150, P240, P360, P500, P600, P800, P1000, P1500, and P2000), and polished with diamond suspensions (6, 1 and $\frac{1}{4}$ μm diamond particles). The etching of the hard-faced layer was done by Aqua Regia (17% HNO_3 , 50% HCl in glycerol), while the base metal was etched with Nital (3% HNO_3 in ethanol). Image analysis was done by ImageJ software. Furthermore, a JEOL JSM6460LV (JEOL, Tokyo, Japan) scanning electron microscope (SEM) equipped with Oxford Instruments INCA Microanalysis system EDS was used to evaluate the composition of different phases. Previously, metallographic specimens were coated with gold by a Ball-Tech Leica SCD-005 (Leica – Leitz, Wetzlar, Germany) device.

The HV5 Vickers hardness measurement was done according to ISO 6507-1:2005 on a VPM HPO 250 (VPM, Rauenstein, Germany) device, with a dwell time of 15 s. A hardness test was conducted in line from the specimen surface to the steel base material, with the distance between indentations of 0.5 mm. Five parallel linear measurements were done on each specimen, with the average value reported.

3. Results

3.1. Hardness Profiles

The results showing hardness profiles of hard-faced layers are shown in Figure 1. In all hard-faced specimens, hardness trends are similar, with values decreasing as the depth of the measurement is higher towards the nickel interlayer and finally the base metal. At a 5 mm distance from the surface, all hardness values reach a similar value which is the hardness of the base metal. There are several differences between the hardness profiles of tested specimens. The maximum hardness near the surface of the specimen 4 is the highest of all tested. Furthermore, the drop of hardness from the surface to the base metal is more pronounced in the specimen 1, hard-faced with unmodified electrodes.

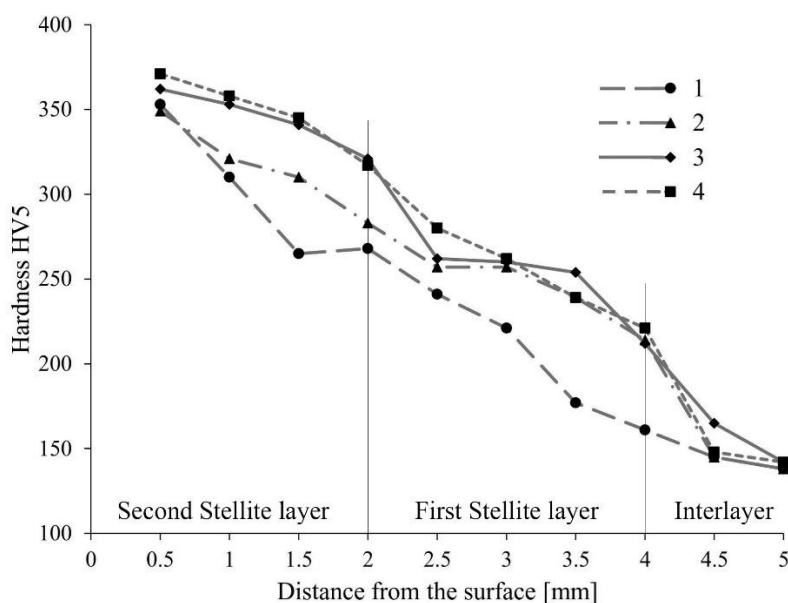


Figure 1. Hardness profiles of layers obtained with unmodified and modified electrodes.

3.2. Wear

The wear rate in the form of mass loss is shown in Figure 2. The coarser abrasive paper and a higher loading result in an increased mass loss of the hard-faced layer, which was expected. The modification of the electrodes by TiO₂ generally results in increased wear resistance of the resulting hard-faced layer, compared to the hard-faced layer obtained with unmodified electrodes. The general trend is that the mass loss is lower, that is, wear resistance is higher as the immersion time is longer. In other words, the advantage of the electrodes treated at longer times is higher as the abrasive grains are larger and as the loading is higher. This indicates that the nanoparticle coating on the electrode is beneficial for increased wear resistance of the hard-faced Stellite alloy.

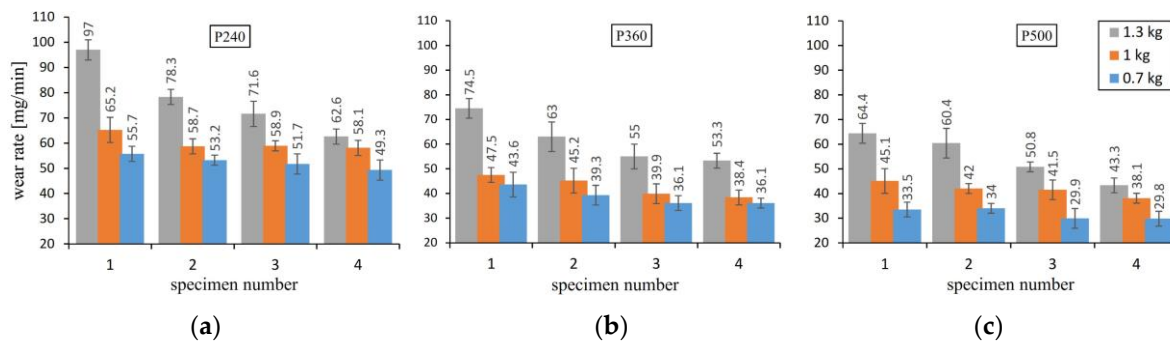


Figure 2. Pin-on-disc wear test results with the following SiC grit sizes: (a) P240; (b) P360; (c) P500

3.3. Microstructure

The microstructures obtained with the light microscope are given in Figures 3 and 4. Figure 3 depicts the microstructures of the hard-faced layer of different specimens, obtained with non-modified (1) and modified (2, 3, 4) at the surface, 1.5 mm under the surface, and 2.5 mm under the surface of the specimen. In all specimens, a typical microstructure consisting of the cobalt-based matrix and eutectic carbides typical for Stellite alloys is present.

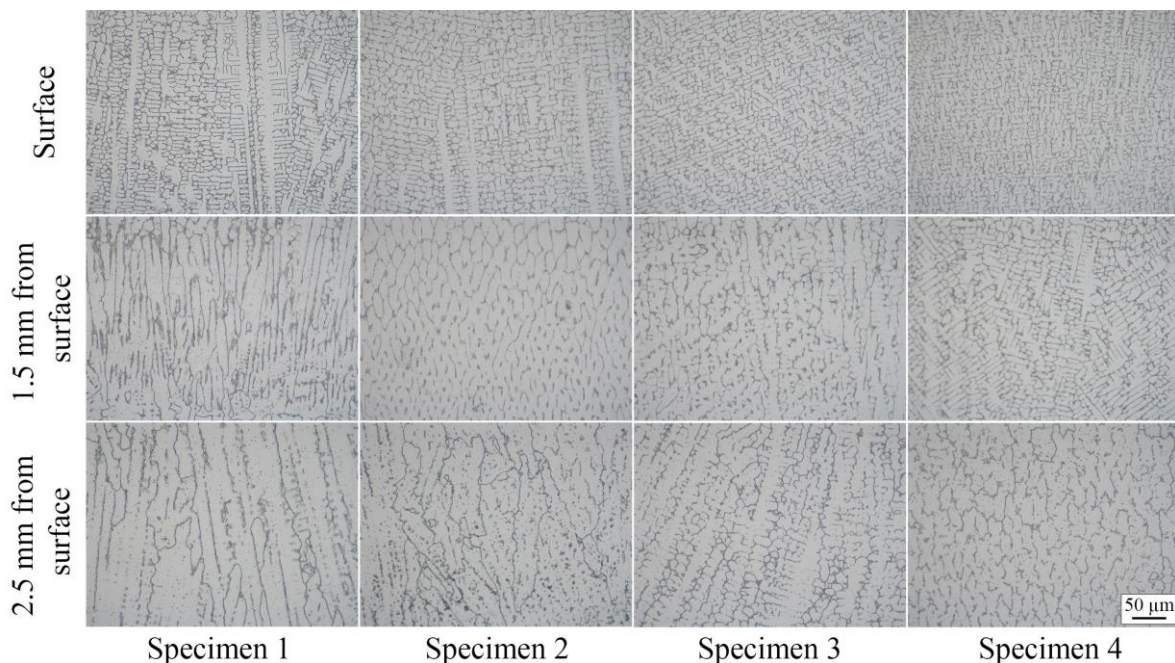


Figure 3. Microstructures of the hard-faced layer of different specimens at different depths.

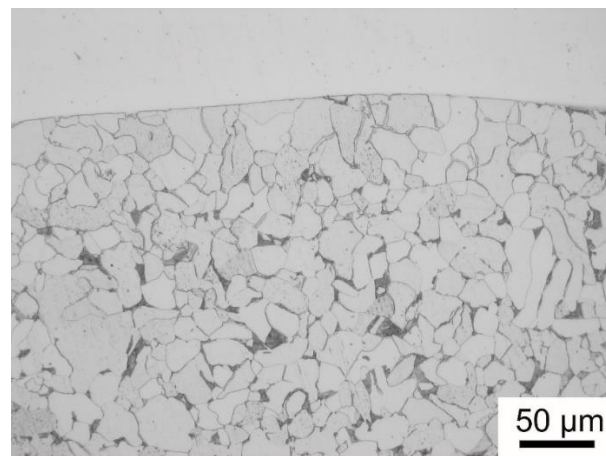


Figure 4. Microstructure of the S235JR base material near the fusion line.

In the surface layer, the interdendritic distance is higher in the hard-faced specimen obtained with untreated consumables (specimen 1) than those obtained with treated ones (specimens 2, 3, 4). Also, the carbide network in specimen 1 is opened to a higher extent than in other specimens, especially the specimen 4, where it is almost completely closed.

A typical cast dendritic primary microstructure morphology gradually becomes less pronounced in terms of the presence of interdendritic phases as the depth is increased. Interdendritic phases morphology becomes gradually changed from a typical interdendritic form to an intergranular and isolated form as the depth increases. However, this transition does not appear to be equal in all specimens. The most pronounced transition is in the specimen 1, obtained with unmodified electrodes.

The results shown in Table 6 reveal that the interdendritic phase (dark areas) volume fraction becomes lower as the depth is increased, which is in accordance with microstructures given in Figure 3. Also, the volume fraction of the interdendritic phases in the specimen hard-faced with treated electrodes is notably smaller than those in specimens hard-faced with treated electrodes, the highest being in specimen 4.

Table 6. Interdendritic phase (dark areas) volume fraction in microstructure.

Specimen	Interdendritic Phase Volume Fraction [%]		
	Surface	1.5 mm under the Surface	2.5 mm under the Surface
1	12.0	11.5	7.9
2	12.3	12.0	10.3
3	12.5	12.1	10.1
4	14.0	12.4	11.0

The microstructure of the base metal is typical for S235JR steel, with slight recrystallization at the fusion line, as shown in Figure 4. Such behavior is noted for all tested specimens.

3.4. EDS Analysis

The results of the EDS analysis are shown in Figures 5 and 6. In Figures 5 and 6, the EDS analyses were done in the area near the surface of the hard-faced layer of specimens 1 and 4, respectively. The interdendritic carbides in specimen 1 belong to the M_7C_3 type of the complex nature (Cr–W) with predominant chromium content, while the matrix is Co-based, as shown in Figure 5. However, in specimen 4, there are also islands that besides the elements detected in specimen 1, contain titanium and oxygen, most probably of titanium-oxide nature. The matrix in specimen 4 has a similar chemical composition as the one in specimen 1, indicating that the matrix does not undergo modification related to chemical content in the presence of nanoparticles.

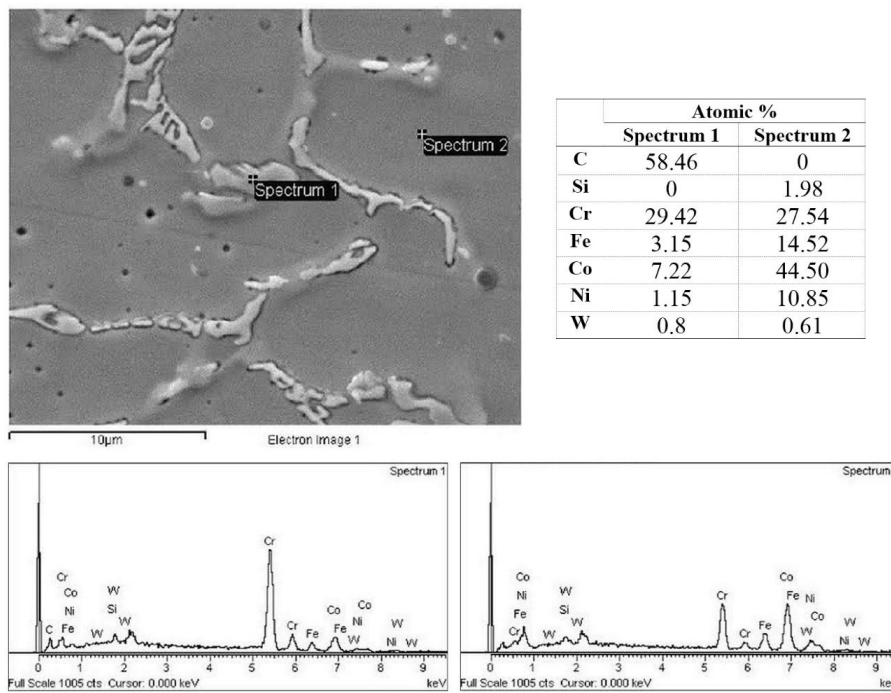


Figure 5. EDS analyses of carbides and base metal in the untreated specimen 1.

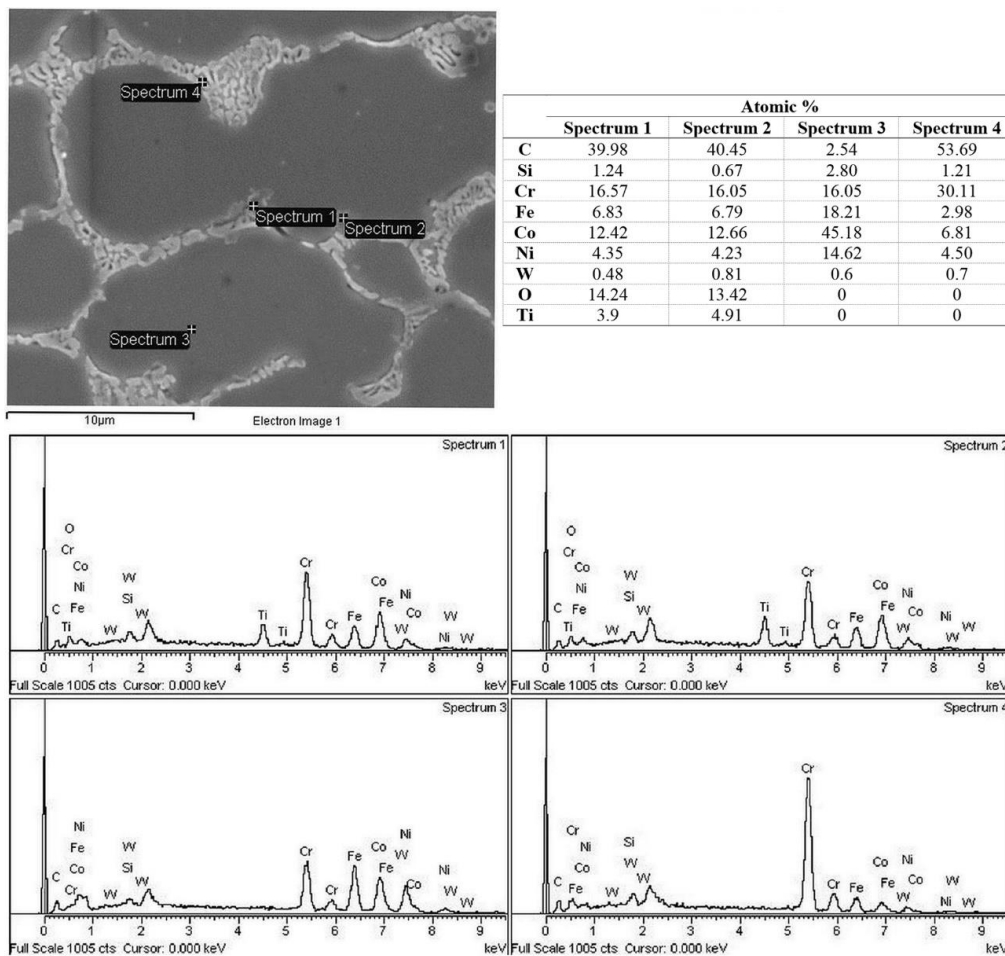


Figure 6. EDS analyses of oxides, carbides and base metal in specimen 4 obtained with electrode treated with TiO₂ nanoparticles (10 mm immersion).

4. Discussion

In this paper, the immersion technique was used to create an additional coating consisting of TiO₂ for increasing the performance of SMAW electrodes for cobalt alloy hard facing, more specifically Stellite 6.

The addition of nanoparticle-based coating to the existing SMAW electrode results in an increased abrasive wear resistance for all hard-faced specimens obtained with modified electrodes. This can be attributed to several effects. The first effect is the occurrence of oxides, the second the decreased interdendritic distance, and the third is the increase in hardness in the surface and subsurface layers. The increase in hardness can also be correlated to the occurrence of titanium-oxides [18–20]. These oxides occur in the form of blocky structures, usually between the Co-based matrix and the complex M₇C₃ chromium-based carbides. Titanium-oxides add to the wear resistance of the resulting hard-faced layer. During welding, a relatively high temperature is developed, sufficient to cause the dissociation of TiO₂ in accordance with the following chemical reaction:



After cooling, the oxygen again tends to form oxides, primarily with Ti. As shown in [15], their solidification temperatures are relatively high: Ti₂O₃ 2130 °C; TiO₂ 1843 °C [21]. A common effect was noticed in cellulose and rutile electrode weldments where similarly modified electrodes influenced the increased inoculation of acicular ferrite through the mechanism of an increased inclusion formation [15,22–26]. However, in this case, the solidification continues with dendritic inoculation and growth.

During cooling, dendrites (Co-alloy forming the metal matrix) solidify second, after titanium oxides at 1475 °C. Finally, the complex (predominantly chromium) carbides of M₇C₃ type are left to solidify the last at 1175 °C [27], forming the microstructure that defines the hard-faced layer obtained with the modified electrodes. This can explain the more random orientation of dendrites shown in Figures 3d and 4d (specimen 4) compared to the specimen 1 obtained with the unmodified electrode. Thus, titanium-oxides have multiple effects, beginning with increasing the hardness both at the specimen surface and in depth, as well as decreasing the interdendritic distance, making the carbide network finer, causing a more effective dispersion strengthening of the matrix, as explained in [28,29].

The increase in wear resistance by adding a TiO₂ nanoparticle coating to the electrodes can influence the increase in wear resistance of the hard-faced layer. This is beneficial from the point of view of CRMs since the hard-faced layer contains cobalt as a basis, tungsten, silicon metal, and molybdenum, as well as near-CRM such as chromium and expensive materials such as nickel. Increased wear resistance can influence the reduction in consumption of these elements, lowering the dependence on them.

5. Conclusions

Based on the results shown in this work, the following conclusions can be drawn:

- The hardness values of hard-faced layers obtained with TiO₂ nanoparticle coating on the SMAW electrode are higher than those of the layers obtained with untreated electrodes.
- The drop of hardness towards the depth of the hard-faced layer is less pronounced in layers obtained with nanoparticle coated electrodes.
- The wear resistance of layers obtained with nanoparticle coatings is increased compared to specimens obtained with unmodified electrodes.
- The highest wear resistance was obtained with electrodes immersed for the longest period of time, 10 min. This effect can be observed for all tested abrasive grain sizes (P240–P500) and loadings (0.7–1.3 kg). The most pronounced increase in wear resistance was when coarser grains at higher loadings were applied.

- Several effects influence the increase in wear resistance: the formation of blocky titanium-oxides, the rise in carbide and oxide volume fraction, and the refinement of dendrites. The dendrite network becomes almost completely closed which can also be one of the effects beneficial for the increase in wear.
- The increased wear resistance of specimens obtained with modified electrodes influence the prolonged life of the component, which can provide significant savings in CRMs such as cobalt, tungsten, molybdenum, and silicon metal, present in the hard-faced alloy.

Author Contributions: Conceptualization, methodology and writing S.B.; investigation P.J. and M.D.; investigation D.L.Z.; formal analysis B.P.; review and editing P.H. and L.J.

Funding: This research received no external funding.

Acknowledgments: This article is based on work from COST Action “Solutions for Critical Raw Materials under Extreme Conditions”, supported by COST (European Cooperation in Science and Technology).

Conflicts of Interest: The authors declare no conflict of interest.

References

1. Haynes, E. Metal Alloy. U.S. Patent No. 873,745, 17 December 1907.
2. Drapier, J.M.; Davin, A.; Magnee, A.; Coutsouradis, D.; Habraken, L. Abrasion and corrosion resistant cobalt base alloys for hardfacing. *Wear* **1975**, *33*, 271–282. [[CrossRef](#)]
3. Wood, P.D.; Evans, H.E.; Ponton, C.B. Investigation into the wear behaviour of Stellite 6 during rotation as an unlubricated bearing at 600 °C. *Tribol. Int.* **2011**, *44*, 1589–1597. [[CrossRef](#)]
4. Gholipour, A.; Shamanian, M.; Ashrafizadeh, F. Microstructure and wear behaviour of Stellite 6 cladding on 174 PH stainless steel. *J. Alloys Compd.* **2011**, *509*, 4905–4909. [[CrossRef](#)]
5. Da Silva, W.S.; Souza, R.M.; Mello, J.D.B.; Goldenstein, H. Room temperature mechanical properties and tribology of NICRALC and Stellite casting alloys. *Wear* **2011**, *271*, 1819–1827. [[CrossRef](#)]
6. Berns, H. Microstructural properties of wear-resistant alloys. *Wear* **1995**, *181*, 271–279. [[CrossRef](#)]
7. Yao, M.X.; Wu, J.B.C.; Xu, W.; Liu, R. Metallographic study and wear resistance of a high-C wrought Co-based alloy Stellite 706K. *Mater. Sci. Eng. A Struct.* **2005**, *407*, 291–298. [[CrossRef](#)]
8. Davis, J.R. *Nickel, Cobalt, Their Alloys*; ASM International: Cleveland, OH, USA, 2001.
9. Exocor Data Sheet. Available online: <http://exocor.com> (accessed on 10 August 2019).
10. Kennametal Data Sheet. Available online: <https://kennametal.com> (accessed on 10 August 2019).
11. Deloro Stellite 6 Data Sheet. Available online: <http://www.deloro.com> (accessed on 14 February 2017).
12. Yao, M.X.; Wu, J.B.C.; Xie, Y. Wear, corrosion and cracking resistance of some W- or Mo-containing Stellite hardfacing alloys. *Mater. Sci. Eng. A Struct.* **2005**, *407*, 234–244. [[CrossRef](#)]
13. Marques, F.P.; Bozzi, A.C.; Scandian, C.; Tschiptschin, A.P. Microabrasion of three experimental cobalt-chromium alloys: Wear rates and wear mechanisms. *Wear* **2017**, *390*, 176–183. [[CrossRef](#)]
14. Luisa Grilli, M.; Bellezze, T.; Gamsjäger, E.; Rinaldi, A.; Novak, P.; Balos, S.; Piticescu, R.R.; Letizia Ruello, M. Solutions for critical raw materials under extreme conditions: A review. *Materials* **2017**, *10*, 285. [[CrossRef](#)] [[PubMed](#)]
15. Report on Critical Raw Materials for EU, Report of the Ad-Hoc Working Group on Defining Critical Raw Materials for EU. May 2014. Available online: <http://mima.geus.dk/report-on-critical-raw-materialsen.pdf> (accessed on 28 August 2019).
16. Balos, S.; Sidjanin, L.; Dramicanin, M.; Labus Zlatanovic, D.; Pilic, B.; Jovicic, M. Modification of cellulose and rutile welding electrode coating by infiltrated TiO₂ nanoparticles. *Met. Mater. Int.* **2016**, *22*, 509–518. [[CrossRef](#)]
17. Balos, S.; Dramicanin, M.; Labus Zlatanovic, D.; Sidjanin, L. SMAW welding aided by TiO₂ nano particles. In Proceedings of the 3rd IIW Sout-East European Welding Congress, Timisoara, Romania, 3–5 June 2015; pp. 1–6.
18. Balos, S.; Dramicanin, M.; Labus Zlatanovic, S.; Sidjanin, L.; Pilic, B. Rutile Electrodes Enhanced with TiO₂ nanoparticles. In *Advanced Materials Research*; Trans Tech Publications: Timisoara, Romania, 2016; pp. 69–74.

19. Fattahi, M.; Nabhani, N.; Vaezi, M.R.; Rahimi, E. Improvement of impact toughness of AWS E6010 weld metal by adding TiO₂ nanoparticles to the electrode coating. *Mater. Sci. Eng. A Struct.* **2011**, *528*, 8031–8039. [[CrossRef](#)]
20. Byun, J.-S.; Shim, J.-H.; Suh, J.-Y.; Oh, Y.-J.; Cho, Y.W.; Shim, J.-D.; Lee, D.N. Inoculated acicular ferrite microstructure and mechanical properties. *Mater. Sci. Eng. A Struct.* **2011**, *319*, 326–331.
21. Greenwood, N.; Earnshaw, A. *Chemistry of the Elements*, 2nd ed.; Butterworth-Heinemann: Woburn, UK, 1997; pp. 961–962.
22. Hossein Nedjad, S.; Farzaneh, A. Formation of fine intragranular ferrite in cast plain carbon steel inoculated by titanium oxide nanopowder. *Scr. Mater.* **2007**, *57*, 937–940. [[CrossRef](#)]
23. Kiviö, M.; Holappa, L.; Jung, T. Addition of dispersoid titanium oxide inclusions in steel and their influence on grain refinement. *Metall. Mater. Trans. B* **2010**, *41*, 1194–1204. [[CrossRef](#)]
24. St-Laurent, S.; L'Esperance, G. Effects of chemistry, density and size distribution of inclusions on the nucleation of acicular ferrite of C-Mn steel shielded-metal-arc-welding weldments. *Mater. Sci. Eng. A Struct.* **1992**, *149*, 203–216. [[CrossRef](#)]
25. Zhang, D.; Terasaki, H.; Komizo, Y. In situ observation of the formation of intragranular acicular ferrite at non-metallic inclusions in C-Mn steel. *Acta Mater.* **2010**, *58*, 1369–1378. [[CrossRef](#)]
26. Byun, J.S.; Shim, J.H.; Cho, Y.W. Influence of Mn on microstructural evolution in Ti-killed C-Mn steel. *Scr. Mater.* **2003**, *48*, 449–454. [[CrossRef](#)]
27. Davis, J.R. *Alloying: Understanding the Basics*; ASM International: Cleveland, OH, USA, 2001.
28. Smallman, R.; Bishop, R.J. *Modern Physical Metallurgy and Materials Engineering*, 6th ed.; Butterworth Heinemann: Woburn, UK, 1999.
29. Sun, N.; Apelian, D. Friction stir processing of aluminum cast alloys for high performance applications. *JOM* **2011**, *63*, 44–50. [[CrossRef](#)]



© 2019 by the authors. Licensee MDPI, Basel, Switzerland. This article is an open access article distributed under the terms and conditions of the Creative Commons Attribution (CC BY) license (<http://creativecommons.org/licenses/by/4.0/>).